GEOPHYSICS, VOL. 80, NO. 1 (JANUARY-FEBRUARY 2015); P. A7–A11, 3 FIGS.
10.1190/GEO2014-0408.1

Internal multiple prediction and removal using Marchenko autofocusing and seismic interferometry

Giovanni Angelo Meles[1], Katrin Löer[1], Matteo Ravasi[1], Andrew Curtis[1], and Carlos Alberto da Costa Filho[1]

ABSTRACT

Standard seismic processing steps such as velocity analysis and reverse time migration (imaging) usually assume that all reflections are primaries: Multiples represent a source of coherent noise and must be suppressed to avoid imaging artifacts. Many suppression methods are relatively ineffective for internal multiples. We show how to predict and remove internal multiples using Marchenko autofocusing and seismic interferometry. We first show how internal multiples can theoretically be reconstructed in convolutional interferometry by combining purely reflected, up- and downgoing Green's functions from virtual sources in the subsurface. We then generate the relevant up- and downgoing wavefields at virtual sources along discrete subsurface boundaries using autofocusing. Then, we convolve purely scattered components of up- and downgoing Green's functions to reconstruct only the internal multiple field, which is adaptively subtracted from the measured data. Crucially, this is all possible without detailed modeled information about the earth's subsurface. The method only requires surface reflection data and estimates of direct (nonreflected) arrivals between subsurface virtual sources and the acquisition surface. The method is demostrated on a stratified synclinal model and shown to be particularly robust against errors in the reference velocity model used.

INTRODUCTION

Many standard seismic data processing steps use the single-scattering Born approximation, and therefore require that multiples are removed from data in advance to avoid errors. Examples include velocity analysis (Yilmaz, 2001; Malcolm et al., 2007) and imaging reflectors using standard linear migration (Zhu et al., 1998; Gray et al., 2001). Surface-related multiples particularly impact on seismic images resulting from marine data, and much effort has been devoted to their removal (see the review by Dragoset et al., 2010). Internal multiples strongly affect land and some marine data, but relatively fewer techniques exist to predict and remove them from reflection data.

Berkhout and Verschuur (1997) iteratively extrapolate shot records to successive reflecting boundaries responsible for multiple generation. Jakubowicz (1998) uses combinations of three observed reflections to predict and remove multiples, leading to several other variations on that theme (e.g., Behura and Forghani, 2012; Hung and Wang, 2012). However, the above schemes require significant prior information about subsurface reflectors or reflections prior to multiple prediction and removal. Inverse scattering methods for multiple prediction (e.g., Weglein et al., 1997, 2003) do not demand so much information but tend to be relatively computationally expensive.

Seismic interferometry techniques synthesize Green's functions among real source or receiver locations by integrating crosscorrelations or convolutions of wavefields recorded by receivers or emanating from sources located elsewhere (Wapenaar, 2004; van Manen et al., 2005, 2006; Wapenaar and Fokkema, 2006; Slob and Wapenaar, 2007). Marchenko autofocusing estimates up- and downgoing components of Green's functions between virtual (imagined) source locations inside a medium and real receivers at the surface (Broggini et al., 2012; Wapenaar et al., 2012, 2013). In contrast to interferometry, autofocusing requires an estimate of the direct wave from the virtual source, illumination only from one side of the medium, and no physical receivers inside the medium.

In principle, autofocused Green's functions provide multiple-free images directly (Behura et al., 2014; Broggini et al., 2014).

Manuscript received by the Editor 26 August 2014; revised manuscript received 24 September 2014; published online 24 December 2014.
[1]The University of Edinburgh, School of GeoSciences, Grant Institute, The King's Buildings, Edinburgh, UK. E-mail: gmeles@ed.ac.uk; k.loer@sms.ed.ac.uk; m.ravasi@sms.ed.ac.uk; andrew.curtis@ed.ac.uk; c.costa@ed.ac.uk.

However, this approach requires as many virtual sources as image points in the subsurface and very large deconvolutional operations. It is thus computationally feasible only if we wish to image a small portion of the subsurface. Autofocusing also allows one to perform Marchenko redatuming of reflectivity to a finite number of depth levels and apply standard imaging in between these redatuming levels (Wapenaar et al., 2014). In this case, however, the redatumed reflectivities do include internal multiples generated from reflectors located below the redatumed level. Our method creates multiple-free data using a relatively small number of virtual sources and no deconvolution.

METHOD

Convolutional interferometry uses acoustic reciprocity theorems to express the Green's function among two locations (van Manen et al., 2005):

$$G(x_2,x_1) = \int_S \frac{1}{\rho(x)}\{G(x_2,x)n_i\partial_i G(x_1,x) - n_i\partial_i G(x_2,x)G(x_1,x)\}\mathrm{d}S \qquad (1)$$

where $\rho(x)$ denotes density, x_1 and x_2 are two receiver (source) positions, $G(x_2,x_1)$ represents the frequency-domain Green's function recorded at x_2 for an impulsive source at x_1, S is an arbitrary boundary of sources (receivers) enclosing either x_1 or x_2, and n_i and ∂_i represent the ith Cartesian component of the normal vector to S and of the gradient, respectively (Figure 1a). We use Einstein summation over repeated indices.

The main contributions to the evaluation of such interferometric surface integrals come from neighborhoods of points of stationary phase of the integrand (Snieder et al., 2006). For some example internal (primary or multiple) reflections, these points are indicated in Figure 1b and 1c. For the geometries considered here, these stationary points are located inside the medium, and usually the corresponding Green's functions in the integrand ($G(x_1,x)$ and $G(x_2,x)$) can be neither measured directly nor modeled accurately. Nevertheless, autofocusing estimates all such Green's functions and their up- and downgoing components at points x (Figure 1d), given only surface reflection data and an estimate of the direct (nonreflected) wavefield from x to the surface (Broggini et al., 2012; Wapenaar et al., 2012, 2013).

Figure 1b and 1c illustrates how primary and internal multiple reflections are reconstructed in convolutional interferometry: Equation 1 essentially pieces together and integrates energy traveling upward and downward from around each stationary point, to calculate energy that would travel along each full raypath. The number of reflections (or scattering order) undergone by an event associated with $G(x_2,x_1)$ is equal to the sum of the number of reflections undergone by its constitutive components, namely, $G(x_1,x)$ and $G(x_2,x)$. Therefore, one component of primaries (scattering order = 1) must be a direct wave (Figure 1b); in contrast, internal multiples can be constructed from reflected waves alone, provided that part of the integration boundary lies between the reflecting interfaces (Figure 1c).

This difference can be used to estimate the internal multiple wavefield. If we remove the direct waves from the Green's functions $G(x_i,x)$ obtained by autofocusing and we use an appropriately restricted integration boundary (e.g., the neighborhood of each stationary point indicated by a square on S_2 in Figure 1d), equation 1 only constructs internal multiples because the integral combines only pairs of reflected waves from x, involving no direct waves. Removing the direct waves from $G(x_i,x)$ is therefore equivalent to considering only stationary points indicated by squares in Figure 1.

Henceforth, we consider partial boundaries consisting of only horizontal lines (Figure 1d) and purely scattered Green's functions (without direct waves), explicitly decomposed into up- and downgoing components. Derivatives in equation 1 are then all vertical. The choice of horizontal boundaries is not mandatory, but it simplifies explanation of the method.

Two combinations of up- and downgoing Green's functions construct the internal multiple shown (those around the stationary black and white squares in Figure 1d). These two contributions would cancel if summed due to the differing directionalities of the corresponding components $G(x_1,x)$ and $G(x_2,x)$. We therefore revise equation 1 using opposite signs for up-down and down-up combinations:

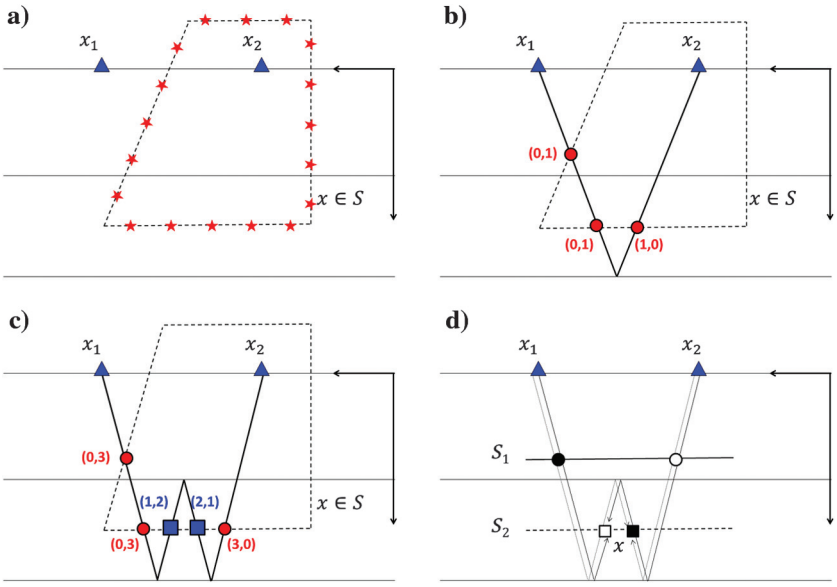

Figure 1. (a) Geometric configuration for convolutional interferometry. Triangles are receivers, and stars are sources. (b and c) Distribution of stationary points for primary and internal multiple reflections, respectively. Circles indicate points $\mathbf{x}$ involving direct and scattered waves, and squares indicate points involving only scattered waves. The scattering order of $\mathbf{G}(\mathbf{x_1},\mathbf{x})$ and $\mathbf{G}(\mathbf{x_2},\mathbf{x})$, i.e., the number of reflections undergone by the corresponding waves, is indicated between brackets for the various stationary points. (d) No stationary point involving purely scattered waves is located along the partial boundary S_1: The downgoing or the upgoing components associated with the corresponding stationary points (black and white circles, respectively) are direct waves. The white square indicates the stationary point along the partial boundary S_2 involving up- and downgoing waves in $\mathbf{G^S}(\mathbf{x_1},\mathbf{x})$ and $\mathbf{G^S}(\mathbf{x_2},\mathbf{x})$, respectively. The black square indicates the stationary point along the partial boundary S_2 involving down- and upgoing waves in $\mathbf{G^S}(\mathbf{x_1},\mathbf{x})$ and $\mathbf{G^S}(\mathbf{x_2},\mathbf{x})$, respectively.

$$G_{\mathrm{IM}}(x_1,x_2) \approx \int_{S_i}\frac{1}{\rho(x)}\{G_u^S(x_2,x_1)\partial_z G_d^S(x_1,x)-\partial_z G_u^S(x_2,x)G_d^S(x_1,x)\}\mathrm{d}S - \int_{S_i}\frac{1}{\rho(x)}\{G_d^S(x_2,x_1)\partial_z G_u^S(x_1,x)-\partial_z G_d^S(x_2,x)G_u^S(x_1,x)\}\mathrm{d}S, \quad (2)$$

where G_{IM} stands for the Green's function's internal multiple components, G_u^S and G_d^S are up- and downgoing components of reflected (scattered) Green's functions that are created using autofocusing, and S_i is a partial boundary ($i = 1, 2, \ldots$; see Figure 1d).

Equations 1 and 2 assume impulsive sources for the reflection data and the autofocusing Green's functions. When using data recorded from band-limited sources, we would simply deconvolve the integral result by the source function (Slob and Wapenaar, 2007).

In contrast to some methods cited above (Jakubowicz, 1998; Behura and Forghani, 2012; Hung and Wang, 2012), our method is based on exact representation theorems, and in principle could estimate exact phases of internal multiples. However, inaccuracies in autofocused Green's functions affect the results. Moreover, higher order multiples involve a larger number of stationary points along S_i than lower order multiples (they cross boundaries at more locations) and are therefore predicted with relatively larger amplitudes. Note that each boundary S_i generates only the family of multiples whose scattered components G_u^S and G_d^S meet at stationary points along S_i, and thus varying S_i provides spatial information about the interfaces generating each multiple: In Figure 1d, using S_2 produces the multiple but S_1 does not; hence, one of the generating interfaces must lie between S_1 and S_2.

We thus derive an algorithm to estimate internal multiples only:

1) Choose a horizontal boundary S_i in the subsurface. Locate virtual sources at regularly sampled locations x along this line, and compute corresponding up- and downgoing Green's function $G_{u/d}(x_p,x)$ and their vertical derivatives using autofocusing, in which locations x_p span the surface array.
2) Mute direct waves in the up- and downgoing Green's functions $G_{u/d}(x_p,x)$ to produce $G^S_{u/d}(x_p,x)$.
3) Apply equation 2 to predict internal multiples $G_{IM}(x_q,x_r)$ for all x_q, x_r in the surface array.

We repeat the procedure using S_i located at different depths to predict different families of internal multiples, then stack the results.

NUMERICAL EXAMPLE

We test the algorithm using a 2D varying density, constant velocity ($v = 1500$ m/s) synclinal model (Figure 2a). We compute synthetic surface seismic data with a finite-difference time-domain modeling code and a Ricker source wavelet with a central frequency of 20 Hz, using absorbing boundaries on all sides (thus assuming that surface-related multiples are removed from recorded data).

Arrays of 201 colocated sources and receivers span 3 km at the top of the model (Figure 2a). Autofocusing requires direct waves from each virtual source to the surface array. To test our method's robustness to inaccuracies in direct wave estimates, we compute direct wave traveltimes through a medium of incorrect constant velocity (1650 m/s — a 10% error), then we apply the source wavelet to estimate associated direct waves. Exact implementation of equation 2 requires knowledge of the subsurface density. This information is usually unknown so we approximate $\rho(x)$ by a smooth density model (Figure 2b). This affects the amplitudes of retrieved multiples, but these will be corrected in the adaptive subtraction below. Crosses in Figure 2b correspond to virtual source positions, spanning a total of nine boundaries S_1 to S_9 with 120 virtual sources each. An additional 18 lines with 120 virtual sources each were simulated (one above, one below each S_i) to estimate the corresponding vertical derivatives in equation 2 using finite differences. We then estimate the relevant Green's functions in equation 2 from each virtual source; this accounts for most of the computational cost of our algorithm, after which the internal multiples corresponding to every source gather can be synthesized relatively cheaply.

Figure 3a shows the reflection data from source 101 indicated in Figure 2, whereas Figure 3b shows estimated primaries obtained by adaptively subtracting (Fomel, 2009) the multiples predicted by stacking results from boundaries S_1 to S_9 individually (Figure 3c). The seven primaries are indicated by dashed lines in Figure 3. Six out of the seven primaries are clearly not reproduced in Figure 3c. The primary corresponding to the fifth reflector (black arrow in Figure 3) seems to be predicted (faintly) as a multiple; this is not an error, but an interesting pathology: In this case, a multiple has exactly the same kinematics as a primary and is correctly recon-

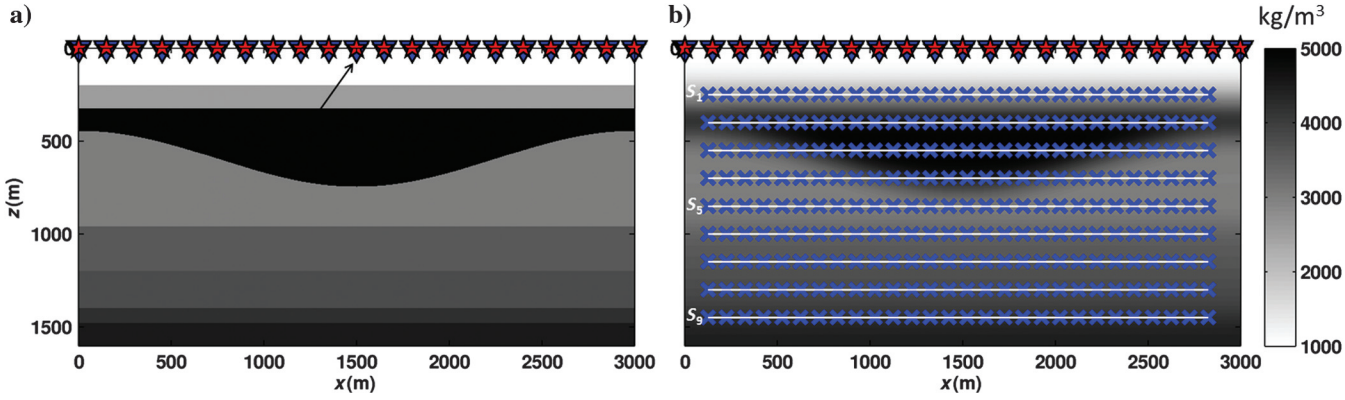

Figure 2. Two-dimensional constant velocity/varying density model. A total of 201 collocated, equally spaced sources and receivers (stars and triangles) are modeled. The black arrow in panel (a) indicates source number 101 used in subsequent figures. (b) Smooth density model used in equations. A total of 1080 virtual sources along nine partial boundaries (crosses and white lines S_1 to S_9) are used in the algorithm.

structed by the method. As expected, the relative amplitudes of the various multiples are different, as some are common to multiple boundaries and are therefore summed multiple times. Nevertheless, all internal multiples are predicted by the algorithm in Figure 3c.

Consider the results from the algorithm using only boundary S_1 or S_2 (Figure 3d and 3e, respectively). In each panel, only a subset of the multiples is retrieved. Moreover, some multiples predicted using boundary S_1 in Figure 3d are not reconstructed using S_2 in Figure 3e. As explained in Figure 1d, this is because the reflectors that generate those missing multiples are either all above or all below boundary S_2. Because S_2 is below S_1, we conclude that those reflectors must all be above S_2. Many events are common to Figure 3d and 3e (specifically those that pass through both boundaries among internal reflections), and some in Figure 3e are not in Figure 3d (those that pass through S_2 but not S_1 among internal reflections). Thus, individual boundaries produce many internal multiples, and variations in results among different boundaries constrain reflector locations.

DISCUSSION

Our method uses autofocusing and a new integral formula to predict multiples with correct phases and only scalar amplitude errors, which may be adaptively subtracted from surface reflection data. Although theoretically it requires as many integration boundaries as there are interfaces in the subsurface, we have also shown that even a single boundary predicts *many* internal multiples (Figure 3d and 3e).

The method requires the removal of direct waves from autofocused Green's functions, which may be challenging for complex models. It may also produce errors due to the partial boundaries and the scattered Green's functions used in equation 2, rather than closed boundaries and complete Green's function in equation 1. Nevertheless, we showed that multiples are predicted remarkably well despite a 10% error in the velocity model used. This is because autofocusing is a time-domain method, and small errors in timing of direct waves result in time shifts of opposite sign in up- and downgoing components. Because these components are convolved, such errors are added, cancel and have little effect on results.

Autofocusing requires an estimate of the direct wavefield at the surface from each subsurface boundary location. Although this is not required by some other schemes (Weglein et al., 1997, 2003; Hung and Wang, 2012), those schemes require an additional assumption of pseudo-depth/-time monotonicity.

Autofocusing may also work in the presence of surface-related multiples (Singh et al., 2014). Our multiple prediction algorithm would then also predict surface-related multiples because the surface simply constitutes another downward-reflecting interface.

CONCLUSION

We presented a new method to predict internal multiples based on autofocusing and convolutional interferometry. The method was demonstrated on acoustic data and proved to be stable with respect to inaccuracies in the autofocused Green's functions. Detailed

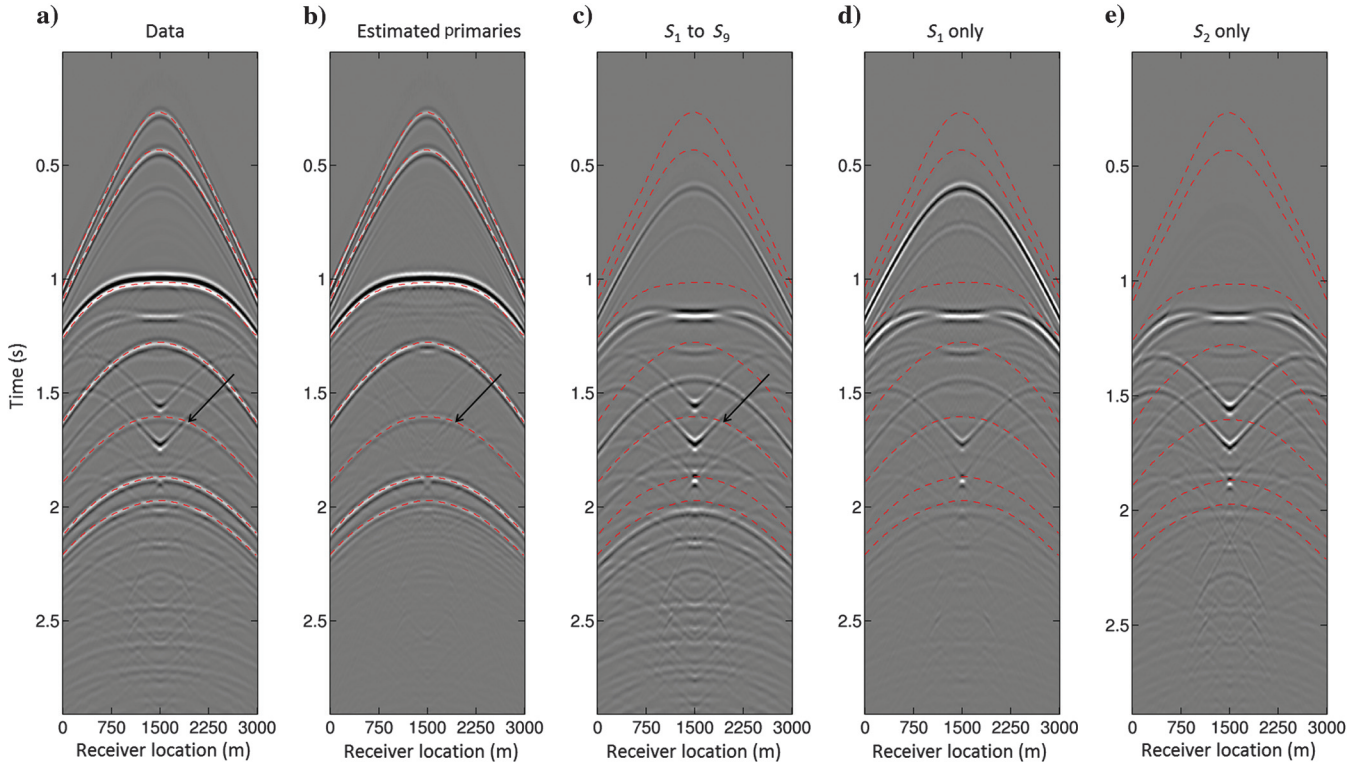

Figure 3. (a) Reflectivity corresponding to source 101 in Figure 2a. Dashed red lines are superimposed on the seven primary reflections. Black arrow indicates the primary corresponding to the fifth interface. A time-varying gain has been applied to enhance later portions of the data. (b) Estimated primaries as obtained by application of adaptive subtraction of internal multiples. (c) Internal multiples predicted using boundaries S_1 to S_9 in Figure 2b. (d and e) Internal multiples predicted using only boundary S_1 and S_2, respectively.

extension of the method to more realistic scenarios will be the topic of future research.

ACKNOWLEDGMENTS

We thank the Edinburgh Interferometry Project (EIP) sponsors (ConocoPhillips, Schlumberger, Statoil, and Total) for supporting this research and J. Robertsson, K. Wapenaar, and an anonymous reviewer for constructive reviews.

REFERENCES

Behura, J., and F. Forghani, 2012, A practical approach to prediction of internal multiples and ghosts: 82nd Annual International Meeting, SEG, Expanded Abstracts, doi: 10.1190/segam2012-1269.1.

Behura, J., K. Wapenaar, and R. Snieder, 2014, Autofocus imaging: Image reconstruction based on inverse scattering theory: Geophysics, **79**, no. 3, A19–A26, doi: 10.1190/geo2013-0398.1.

Berkhout, A. J., and D. J. Verschuur, 1997, Estimation of multiple scattering by iterative inversion, Part I: Theoretical consideration: Geophysics, **62**, 1586–1595, doi: 10.1190/1.1444261.

Broggini, F., R. Snieder, and K. Wapenaar, 2012, Focusing the wavefield inside an unknown 1D medium — Beyond seismic interferometry: Geophysics, **77**, no. 5, A25–A28, doi: 10.1190/geo2012-0060.1.

Broggini, F., R. Snieder, and K. Wapenaar, 2014, Data-driven wave field focusing and imaging with multidimensional deconvolution: Numerical examples for reflection data with internal multiples: Geophysics, **79**, no. 3, WA107–WA115, doi: 10.1190/geo2013-0307.1.

Dragoset, B., E. Verschuur, I. Moore, and R. Bisley, 2010, A perspective on 3D surface-related multiple elimination: Geophysics, **75**, no. 5, A245–A261, doi: 10.1190/1.3475413.

Fomel, S., 2009, Adaptive multiple subtraction using regularized nonstationary regression: Geophysics, **74**, no. 1, V25–V33, doi: 10.1190/1.3043447.

Gray, S., J. Etgen, J. Dellinger, and D. Whitmore, 2001, Seismic migration problems and solutions: Geophysics, **66**, 1622–1640, doi: 10.1190/1.1487107.

Hung, B., and M. Wang, 2012, Internal demultiple methodology without identifying the multiple generators: 82nd Annual International Meeting, SEG, Expanded Abstracts, doi: 10.1190/segam2012-0549.1.

Jakubowicz, H., 1998, Wave equation prediction and removal of interbed-multiples: 68th Annual International Meeting, SEG, Expanded Abstracts, 1527–1530.

Malcolm, A. E., M. V. de Hoop, and H. Calandra, 2007, Identification of image artifacts due to internal multiples: Geophysics, **72**, no. 2, S123–S132, doi: 10.1190/1.2434780.

Singh, S., R. Snieder, J. Behura, J. van der Neut, K. Wapenaar, and E. Slob, 2014, Autofocusing for retrieving the Green's function in the presence of a free surface: 76th Annual International Conference and Exhibition, EAGE, Extended Abstracts, Th E102 09.

Slob, E., and K. Wapenaar, 2007, GPR without a source: Cross-correlation and cross-convolution methods: IEEE Transactions on Geoscience and Remote Sensing, **45**, 2501–2510, doi: 10.1109/TGRS.2007.900995.

Snieder, R., K. Wapenaar, and K. Larner, 2006, Spurious multiples in interferometric imaging of primaries: Geophysics, **71**, no. 4, SI111–SI124, doi: 10.1190/1.2211507.

van Manen, D.-J., A. Curtis, and J. O. A. Robertsson, 2006, Interferometric modeling of wave propagation in inhomogeneous elastic media using time reversal and reciprocity: Geophysics, **71**, no. 4, SI47–SI60, doi: 10.1190/1.2213218.

van Manen, D.-J., J. O. A. Robertsson, and A. Curtis, 2005, Modeling of wave propagation in inhomogeneous media: Physical Review Letters, **94**, 164301, doi: 10.1103/PhysRevLett.94.164301.

Wapenaar, K., 2004, Retrieving the elastodynamic Green's function of an arbitrary inhomogeneous medium by crosscorrelation: Physical Review Letters, **93**, 254301–254304, doi: 10.1103/PhysRevLett.93.254301.

Wapenaar, K., F. Broggini, and R. Snieder, 2012, Creating a virtual source inside a medium from reflection data: Heuristic derivation and stationary phase analysis: Geophysical Journal International, **190**, 1020–1024, doi: 10.1111/j.1365-246X.2012.05551.x.

Wapenaar, K., F. Broggini, E. Slob, and R. Snieder, 2013, Three-dimensional single-sided Marchenko inverse scattering, data-driven focusing, Green's function retrieval, and their mutual relations: Physical Review Letters, **110**, 084301, doi: 10.1103/PhysRevLett.110.084301.

Wapenaar, K., and J. Fokkema, 2006, Green's function representations for seismic interferometry: Geophysics, **71**, no. 4, SI33–SI46, doi: 10.1190/1.2213955.

Wapenaar, K., J. Thorbecke, J. van der Neut, F. Broggini, E. Slob, and R. Snieder, 2014, Marchenko imaging: Geophysics, **79**, no. 3, WA39–WA57, doi: 10.1190/geo2013-0302.1.

Weglein, A., F. Araújo, P. Carvalho, R. Stolt, K. Matson, R. Coates, D. Corrigan, D. Foster, S. Shaw, and H. Zhang, 2003, Inverse scattering series and seismic exploration: Inverse Problems, **19**, R27–R83, doi: 10.1088/0266-5611/19/6/R01.

Weglein, A., F. A. Gasparotto, P. M. Carvalho, and R. H. Stolt, 1997, An inverse-scattering series method for attenuating multiples in seismic reflection data: Geophysics, **62**, 1975–1989, doi: 10.1190/1.1444298.

Yilmaz, O., 2001, Seismic data analysis: Processing, inversion and interpretation of seismic data: SEG.

Zhu, J., L. Lines, and S. Gray, 1998, Smiles and frowns in migration/velocity analysis: Geophysics, **63**, 1200–1209, doi: 10.1190/1.1444420.